

# **Shape fluctuations of a spherical surfactant shell in a microemulsion**

An experiment using the Neutron Spin-Echo Spectrometer

Summer School on Methods and Applications of Neutron Spectroscopy

NIST Center for Neutron Research

June 25-29, 2007

**Antonio Faraone, Jason S. Gardner, and Michihiro Nagao**

## **Abstract**

Using the neutron spin-echo technique, we will investigate the dynamics of the shape fluctuation of microemulsion droplets. From the measured relaxation frequency spectrum we will determine the bending modulus of elasticity of the surfactant film. By means of this experiment, we will illustrate the principles of the neutron spin-echo technique, the required measurements and corrections, and the process of reducing the measured "echoes" to obtain the intermediate scattering function. We aim to a better understanding of the link between structure and dynamics in colloidal fluids.

## **1. Introduction**

Surfactants are amphiphilic molecules in which part of the molecule is hydrophilic (likes water) and part is hydrophobic (fears water); see figure 1. In aqueous solution, surfactants aggregate into structures called micelles. Micelles are closed shape structures where the hydrophilic portions of the molecule are exposed to the surrounding water while the hydrophobic portions are protected from contact with water, as seen in figure 1. When dissolved in non-polar organic solvents (hereafter referred simply as oils), surfactants form reversed micelles where the hydrophilic portions are shielded from contact with the surrounding solvent in the interior of the micelles; see figure 1. Depending on the particular molecular architecture of the surfactant molecule, a variety of microstructures may be formed. Possible aggregate structures are spherical, cylindrical and worm-like micelles, spherical vesicles, lamellar sheets, or a variety of other topologies. The surfactant aggregates form in order to minimize the free energy of the solution. As a result, they are dynamic (but equilibrium) structures, able to rearrange in response

to changing environmental conditions. An interesting property of the micelles is their ability to solubilize certain amount of solute in their interior which otherwise is not soluble in the solvent. For example, if micelles are formed in *n*-hexane, their interior is hydrophilic (because the hydrophilic portions of the surfactant molecules are oriented inward) and small amount of water can be accommodated in the micellar core. As a result, the micelles will swell and their size will increase. If we increase the amount of solubilized phase, the micelles will evolve into a microemulsion (it is called a microemulsion although the droplet size is below 100 nm), which is a thermodynamically stable, isotropic, and optically transparent solution. These systems are of much interest to the industry of detergent and oil recovery.

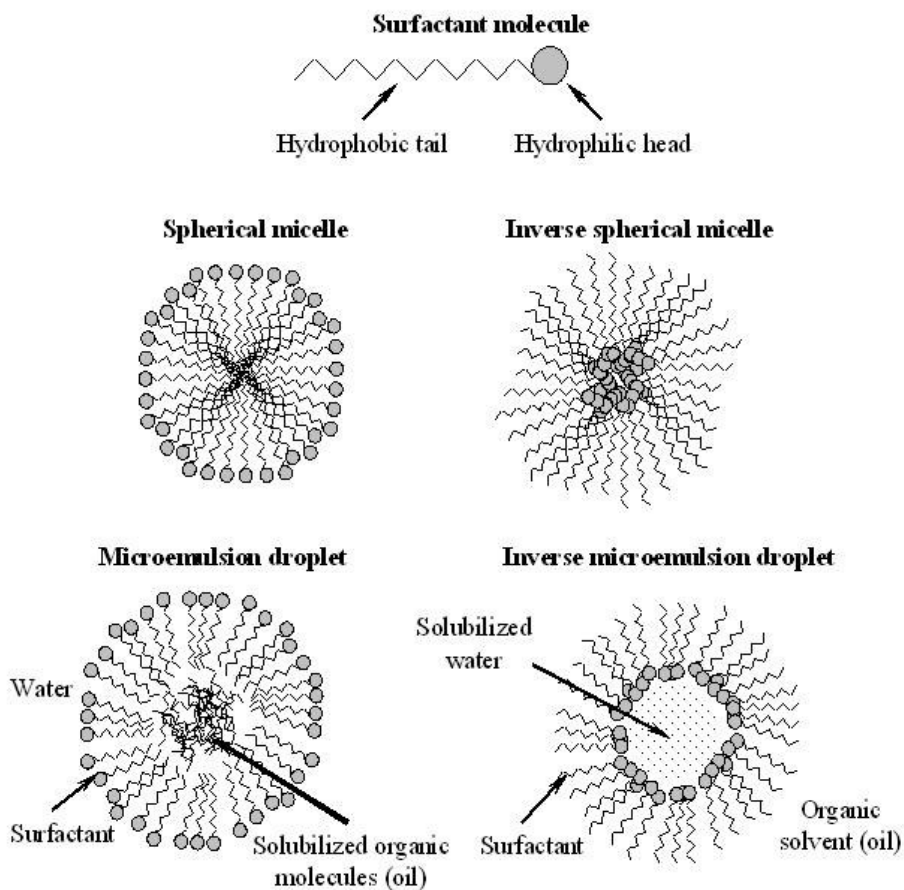


**Figure 1.** Illustration of micelles and microemulsions

In microemulsions, the interfacial surface area is very big, and, therefore it is expected that the properties and structure of the microemulsion will be dependent on the nature of this surfactant layer. In particular, the formation of microemulsion droplets is mainly due to the natural bending tendency of the surfactant layer, the minimization of the bending elastic energy resulting in the observed structure.

The basic idea of the experiment we are going to perform is that thermal fluctuations of the surfactant film distort the droplet from its average (presumably spherical) form. Using the neutron spin-echo (NSE) technique we will measure the relaxation frequency of these small fluctuations. It is important to reduce the scattering volume to the actually fluctuating part, and in this respect [3], we will take full advantage of the contrast matching technique. This is a peculiar feature offered by neutron scattering techniques, in particular small angle.

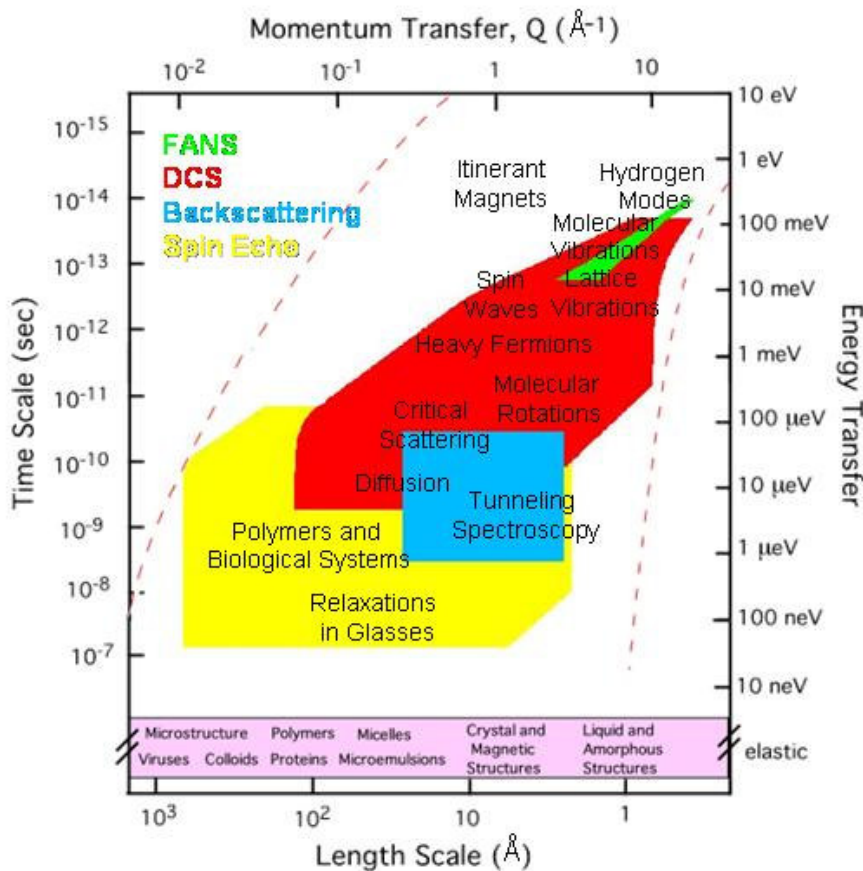


**Figure 2.** Phase space diagram indicating the accessible regions to the high-resolution spectrometers at the NCNR. Many different fields of application of elastic and inelastic neutron scattering are reported as well.

Figure 2 shows the accessible regions of the  $Q$ - $t$  phase space to the three high resolution spectrometer at the NCNR: DCS, HFBS, and NSE. It can be seen that NSE is the instrument able to probe the largest length scale and the longest time scale. As a matter of fact, the NSE technique is substantially different from the conventional inelastic neutron scattering techniques. In fact, it allows for the detection of small velocity changes of the neutrons during the scattering process, in spite of the fact that an incoming polarized beam of 10-20% velocity spread (and

therefore reasonably intense) is used. The trick consists making use of the Larmor precession of the neutron's spin as an 'internal' clock [4]. Since the Larmor precession information on the incoming velocity of each neutron is stored on the neutron itself, it can be compared with the outgoing velocity of one and the same neutron. The basic idea is the following: the precession frequency is controlled by a magnetic field along the flight path from a so called  $\pi/2$ -flipper to the sample. A symmetric setup is placed in the flight path from the sample to a second  $\pi/2$ -flipper. Close to the sample a  $\pi$ -flipper reverse the precession angle such that for an elastically scattered neutron there is no net spin turn at the second  $\pi/2$ -flipper, irrespective of the starting velocity of the neutron. Only if the symmetry is distorted due to a velocity change at the sample the precession angles in the primary and secondary paths of the spectrometer differ, and a polarization change after the second  $\pi/2$ -flipper is observed. Using this set-up is possible to make extremely accurate measurements of the energy change during the scattering process, and therefore design spectrometer with high resolution.

From an inspection of figure 2, it is easy to realize that the NSE spectrometer is the instrument best suited for the investigation of thermal fluctuations in microemulsion droplet. In fact, it allows the investigation of space scale up to the tenths of nanometer and relaxation times from the fraction of nanosecond to one hundred nanoseconds.

## 2. The sample

The sample used for these experiments is the surfactant sodium bis(2-ethylhexyl)-sulfosuccinate (AOT) dissolved in deuterated *n*-hexane (*d*-hexane,  $C_6D_{14}$ ). In hexane, AOT aggregates into nearly spherical micelles of approximate radius of 2 nm. When water is added to the solution it will be encapsulated inside the micelles forming a microemulsion. Mixing 5.1 % by volume of AOT, 2.5 % by volume of  $D_2O$  and 92.4 % by volume of  $C_6D_{14}$  we will obtain that the volume fraction of the droplets is  $\phi_V = 0.076$ . The microemulsion particles can be well described by a core-shell structure where the core is comprised of  $D_2O$  and the shell is formed by the AOT film. Since  $D_2O$  has a scattering length density very similar to that of *d*-hexane, we obtain a film contrast of the microemulsion: mainly the scattering of the surfactant shell will contribute to the recorded spectra.

| Property @ 25°C             | AOT                     | Deuterated <i>n</i> -hexane | Deuterated water      |
|-----------------------------|-------------------------|-----------------------------|-----------------------|
| Formula                     | $C_{20}H_{37}O_7SNa$    | $C_6D_{14}$                 | $D_2O$                |
| MW/ g mol <sup>-1</sup>     | 444.6                   | 100.26                      | 20.0                  |
| Density/ g ml <sup>-1</sup> | 1.13                    | 0.767                       | 1.1                   |
| SLD/ Å <sup>-2</sup>        | $\sim 1 \times 10^{-7}$ | $6.14 \times 10^{-6}$       | $6.35 \times 10^{-6}$ |
| Viscosity/ cP               | -                       | $\sim 0.31$                 | 1.096                 |

**Table 1.** Some important parameters needed for the data analysis

- Do you know how to calculate the scattering length density?

Table 1 reports the principal physical properties of the components of the investigated samples. We will use these parameters during the analysis of our data. A small angle neutron scattering experiment (SANS) will have been performed before the start of the summer school, in order to obtain the structural information needed to determine the bending modulus of elasticity of the AOT film.

### 3. The NSE technique and the spectrometer

Figure 3 shows in detail the manipulation of the neutron spins through the NSE spectrometer. After the neutron beam ( $\Delta\lambda/\lambda=10-20\%$ , depending on the tilt angle of the velocity selector) is polarized in the longitudinal direction by a Mezei cavity, the neutron spins are rotated by  $90^\circ$  by the first  $\pi/2$ -flipper, which begins the precession of the neutron in the field produced by the main coil. In a perpendicular magnetic field  $B_i$ , a neutron spin will undergo precessions at a frequency  $\omega_L = -\gamma_L B_i$ . If a neutron is polarized perpendicularly to a homogeneous field, it will precess through an angle

$$\phi_i = \gamma_L \frac{m\lambda}{h} \int_i B_i(l) dl = \gamma_L \frac{m\lambda}{h} I_i \quad (1)$$

where  $I_i$  is the field integral along solenoid  $i$  and  $\lambda$  is the wavelength of the neutron ( $v=h/m\lambda$  is its velocity). For a beam of neutrons with an incident wavelength distribution  $f(\lambda)$  and  $\langle\lambda\rangle=\langle\lambda_i\rangle$ , each neutron undergoes a spin precession of  $\phi_i(\lambda)$  in the first arm of the spectrometer. The neutron beam, with its broad band of wavelength, will completely depolarize in this first precession field. After scattering from the sample, a neutron passing through the  $\pi$ -flipper will change its phase from  $\phi \bmod(2\pi)$  to  $-\phi \bmod(2\pi)$ . Then, on passing through the second precession field, if the scattering is elastic and the two field integrals are the same, the beam recovers its full polarization at the second  $\pi/2$ -flipper, which rotates the spins back to the longitudinal direction, thereby stopping the precessions.

If the neutrons are scattered quasi-elastically from the sample, changing wavelength by  $\delta\lambda$ , they will undergo a spin precession with phase angle  $\phi_2$  in the second arm of the spectrometer. The phase difference will be:

$$\varphi = \phi_1(\lambda) - \phi_2(\lambda + \delta\lambda) = \phi_1(\lambda) - \phi_1(\lambda + \delta\lambda) + \Delta\phi(\lambda + \delta\lambda) \quad (2)$$

where  $\Delta\phi(\lambda) = \phi_1(\lambda) - \phi_2(\lambda)$ .

To first order in  $\lambda\delta\lambda$  and  $\Delta\phi$ , the phase shift is composed of a term from the inelasticity and a term from the difference in the field integrals (recall that  $\phi \propto \lambda$ ):

$$\varphi = \phi_1(\langle\lambda_1\rangle) \frac{\lambda}{\langle\lambda_1\rangle} - \phi_1(\langle\lambda_1\rangle) \frac{\lambda + \delta\lambda}{\langle\lambda_1\rangle} + \Delta\phi(\langle\lambda_1\rangle) \frac{\lambda}{\langle\lambda_1\rangle} = \frac{\phi_1(\langle\lambda_1\rangle)\delta\lambda + \Delta\phi(\langle\lambda_1\rangle)\lambda}{\langle\lambda_1\rangle} \quad (3)$$

The inelasticity of the scattering can be written as a change in wavelength:

$$\hbar\omega = E_1 - E_2 = \frac{\hbar^2}{2m} \left[ \frac{1}{\lambda^2} - \frac{1}{(\lambda + \delta\lambda)^2} \right] \quad (4)$$

where to the first order in  $\delta\lambda$

$$\hbar\omega = \frac{\hbar^2}{m} \frac{\delta\lambda}{\lambda^3} \quad (5)$$

which connects  $\delta\lambda$  to  $\omega$ .

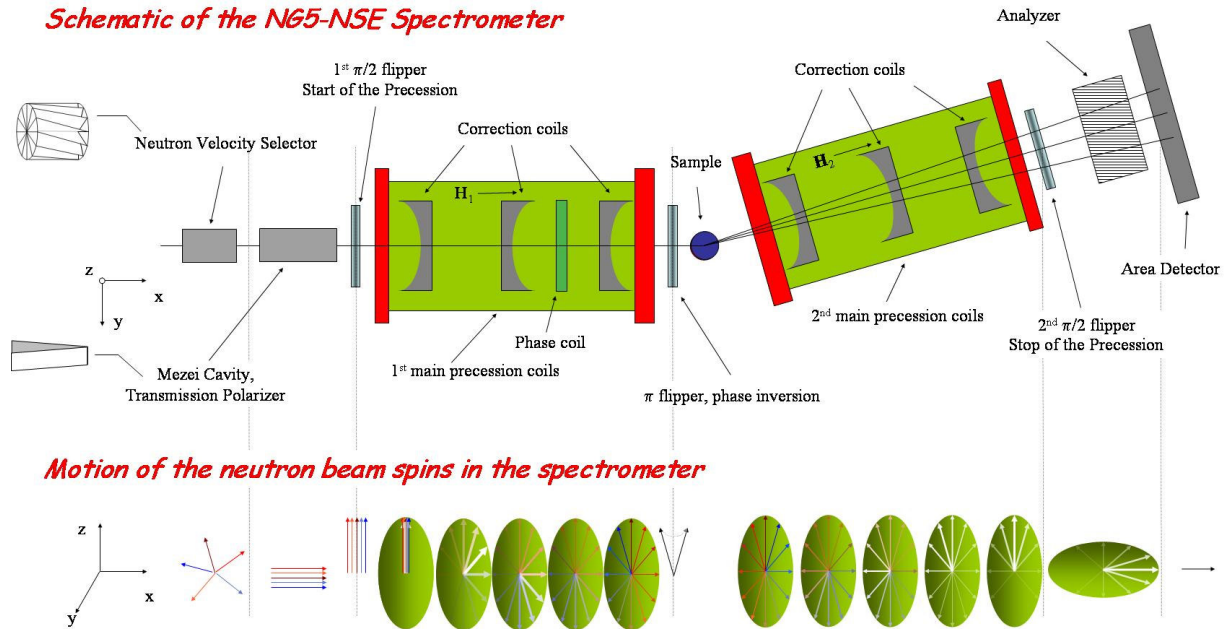


**Figure 3.** Schematic of the NSE spectrometer and motion of the neutron spins looking perpendicular to the beam direction.

Due to the quantum nature of the neutron spin, only one component of the spin, call it  $z$ , can be determined. The polarization of the scattered beam, which is the quantity measured during a NSE experiment, is given by:

$$\langle P_z \rangle = \langle \cos(\phi) \rangle = \int f(\lambda) d\lambda \int S(Q, \omega) \cos \left[ \frac{\phi_1(\langle \lambda_1 \rangle) m \lambda^3 \omega + \Delta\phi(\langle \lambda_1 \rangle) \lambda}{\langle \lambda_1 \rangle} \right] d\omega \quad (7)$$

where we have integrated over the distribution of incoming wavelength and exchanged energies, this latter distribution being defined by the scattering function  $S(Q, \omega)$ .

Since we have assumed  $S(Q, \omega)$  is a quasi-elastic scattering law, which is essentially an even function of  $\omega$ , the cosine can be factorized:

$$\begin{aligned} \langle P_z \rangle &= \int f(\lambda) \cos \left[ \frac{\Delta\phi(\langle \lambda_1 \rangle) \lambda}{\langle \lambda_1 \rangle} \right] d\lambda \int S(Q, \omega) \cos \left[ \frac{\phi_1(\langle \lambda_1 \rangle) m \lambda^3 \omega}{2\pi\hbar \langle \lambda_1 \rangle} \right] d\omega = \\ &\int f(\lambda) \cos \left[ \frac{\Delta\phi(\langle \lambda_1 \rangle) \lambda}{\langle \lambda_1 \rangle} \right] d\lambda \int S(Q, \omega) \cos \omega t_F d\omega \end{aligned} \quad (8)$$

where

$$t_F = \frac{\phi_1(\langle \lambda_1 \rangle) m \lambda^3}{2\pi\hbar \langle \lambda_1 \rangle} = \gamma_L \left( \frac{m}{h} \right)^2 \frac{\lambda^3}{2\pi} I_1 \quad (9)$$

is the Fourier time.

By adjusting the field so that the echo condition is met ( $I_1=I_2$ , i.e.  $\Delta\phi=0$ ), the beam polarization is:

$$\langle P_z \rangle = \int f(\lambda) d\lambda \int S(Q, \omega) \cos \omega t_F d\omega = \int f(\lambda) I(Q, t_F) d\lambda \quad (10)$$

$I(Q, t)$  is the intermediate scattering function, which is the spatial Fourier transform of the van-Hove correlation function  $G(r, t)$  (remember that  $G(r, t)$ , classically, represents the probability that given a particle at the origin at time zero, a particle is at position  $r$  at time  $t$ ,  $G$  is composed of a self,  $G_s(r, t)$  probed by incoherent scattering, and of a distinct part). The scattering function  $S(Q, \omega)$  is the cosine transform of  $I(Q, t)$ . In many experimental cases  $I(Q, t)$  varies slowly with  $\lambda$ , and so it can be removed from the integrand, in these cases, NSE spectroscopy directly measures the intermediate scattering function, not being necessary to determine the wavelength distribution.

The notion ‘‘high resolution’’ used in connection with NSE instruments means high achievable Fourier times. There are two parameters available to influence  $t_F$ : the neutron wavelength and the field integral  $I$ . The former depends on the neutron source characteristics as well as on the desired Q-range. At the NCNR the highest neutron flux is at  $\lambda \approx 6$  Å, in order to reach higher  $t_F$  a price in terms of incoming neutron has to be paid. The field integral depends on the design and characteristics of the spectrometers. Different issues limit its value. Achieving a high value of  $I$  by aiming at a value of the magnetic field  $B$  is limited by the costs and by the unavoidable inhomogeneity of  $I$ , i.e. the differences of  $I$  along different neutron paths have to be

small compared to the value corresponding to half a precession. In order to reduce the inhomogeneities related to the radial variation of the field and to the different path length present in a divergent beam, special correcting elements, the so-called “Fresnel coils”, have to be inserted along the flight path. . Figure 4 shows the resolution of the NCNR NSE spectrometer at different wavelengths, the vertical lines indicate the maximum  $t_F$  achievable at the corresponding wavelengths.

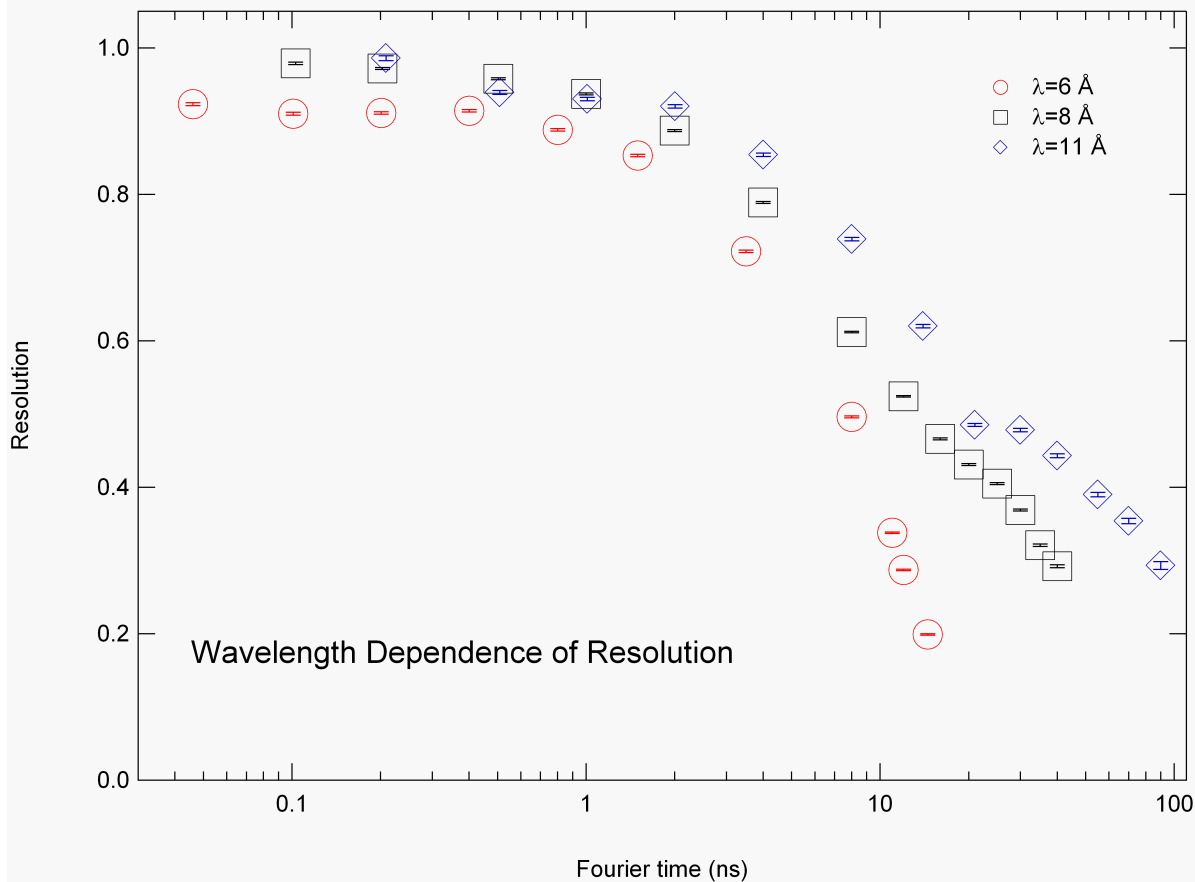


**Figure 4.** Wavelength dependence of the resolution function.

The polarization of the scattered neutrons at the end of the second precession field is detected by an analyzer, made of an array of supermirrors, in front of the detector that transmits only neutrons of one polarization direction. Neutrons are detected by a  $32 \times 32$  cm<sup>2</sup> multidetector with a resolution of 1cm<sup>2</sup>. We will see in the data reduction section how to take full advantage of the multidetector to measure different  $Q$  values at the same time.

A spin-echo measurement is usually performed by setting the spectrometer to the echo condition ( $I_1=I_2$ ), obtaining the intermediate scattering function using equation 10. In practice the counting rate ( $N$ ) is measured for several phase current ( $\phi_c$ ) values near the echo position, then fitted to a Gaussian damped cosine function to give the echo amplitude,  $A$ :

$$N = N_0 + A \exp\left[\frac{(\phi_c - \phi_0)^2}{2\sigma^2}\right] \cos\left[\frac{360}{T}(\phi_c - \phi_0)\right] \quad (11)$$

- Can you explain why equation 11 is used to fit the echo?
- What is the relation between the fitting parameters  $\sigma$  and  $T$  and the incoming wavelength distribution  $f(\lambda)$ ?

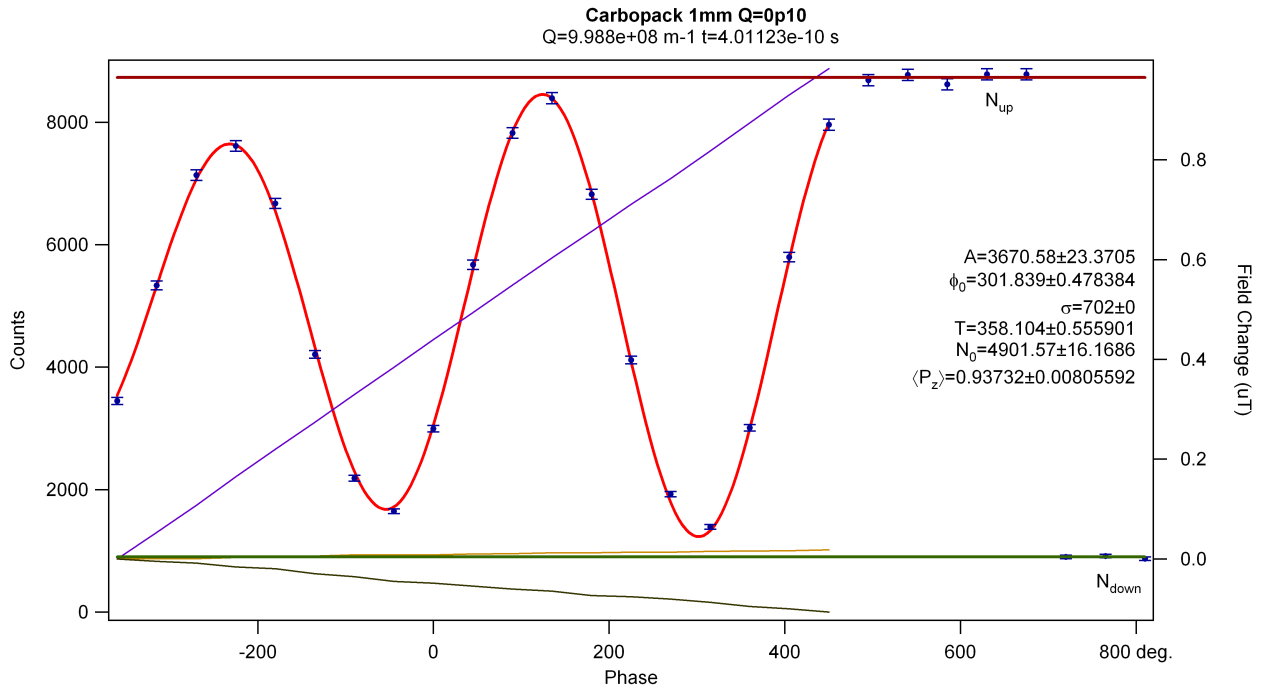


**Figure 5.** NSE signal as a function of the phase difference between the incident and scattered beams. The red curve is the fit according to equation 11 (can you tell why  $\sigma$  is a fix parameter?). The blue, orange, and black lines are the magnetic field along the three orthogonal directions at the sample position. In this way the presence of stray magnetic fields due to the environment can be recorded.

The effect of the less-than-perfect efficiency of the flippers, the polarizer, and the analyzer is removed by measuring the count rates with the  $\pi/2$ -flippers off and the  $\pi$ -flipper both off and on, giving the non spin flip,  $N_{up}$ , and spin flip counts,  $N_{down}$ , respectively. The measured value of the polarization of the scattered beam at the echo point  $\langle P_z \rangle_S$  is given by:

$$\langle P_z \rangle_S = \frac{2A}{N_{up} - N_{down}} \quad (12)$$

Inhomogeneities in the magnetic field may further reduce the polarization. As these inhomogeneities are not correlated with  $S(Q, \omega)$  or  $f(\lambda)$ , their effect may be divided out by measuring the polarization from a purely elastic scatterer:

$$\langle P_z \rangle_E = \frac{2A^E}{N_{up}^E - N_{down}^E} \quad (13)$$

In order to ensure that the dynamic scattering from everything that is not our sample is not contributing, a background measurement must be performed. The sample holder (including the pure solvent, if any) must then be measured, under identical conditions as your sample.

The normalized intermediate scattering function is then obtained by:

$$\frac{I(Q, t)}{I(Q, 0)} = \left[ \frac{2(A - TA^{bgr})}{(N_{up} - N_{down}) - T(1 - \phi_V)(N_{up}^{bgr} - N_{down}^{bgr})} \right] / \frac{2A^E}{N_{up}^E - N_{down}^E} \quad (14)$$

where  $T$  is the ratio of the transmissions of the sample and the background sample, and  $(1 - \phi_V)$  is the volume fraction of the solvent in the sample. Therefore, transmissions of both the sample and the solvent (with respect to an empty beam) must be measured at the respective wavelength, so that the correct fraction of solvent scattering (echo amplitude) can be subtracted.

Experimentally,  $Q$  is determined by the incoming neutrons wavelength and by the scattering angle, the angle between the direct beam and the second arm of the spectrometer. In an NSE experiment it can be measured only the scattering in the direction of the second arm. However, using a multidetector, it is still possible to measure  $I(Q, t)$  at different  $Q$  values (around the mean  $Q$  value, determined by the scattering angle). At the NSE spectrometer of the NCNR, the scattering angle can be varied between  $\approx 2^\circ$  and  $105^\circ$ . The time is varied, according to equation 9, by changing the field in the main coils.

Having measured the scattering function in the time domain, from equation 14 it can be seen that, unlike other spectrometers, the instrumental resolution effects in NSE spectroscopy may be simply divided out by measuring the response of a purely elastic scattering sample. This is a great advantage and spares the user the often complicated task of deconvolving the instrumental energy lineshape from the physical lineshape.

- How do you know if your sample scatters "well" or "good enough"?
- How long do you have to count for each measurement?

#### 4. Data reduction

Data reduction of NSE data is not a straightforward process. This is mostly due to the fact that we want to achieve full benefit from the multidetector. In fact, the echo determination must

be done patch by patch on the detector surface, to take account for the residual phase shifts observed. The pixels are usually binned into areas of 2×2 or 4×4, and then these areas are analyzed individually. This process must be performed very carefully especially for the resolution. It is important that the measured phase varies smoothly on the surface of the detector and that it varies about linearly for each area as a function of the time. This is not always easy, especially near the edge of the detector or at high Fourier times, where the signal-to-noise ratio is not very good. Luckily, once the phases are determined for the resolution samples they can be ‘imported’ for the analysis of the sample itself and of the background.

Finally, data from areas (usually ring segments) representing the same momentum transfer  $Q$  are collected and evaluated into several  $I(Q_i,t)/I(Q_i)$  curves. For this reason we have to accurately measure the position of the beam center.

- Each pixel of the 2-D detector counts neutrons with a slightly different efficiency ( $\pm 10\%$ ). Does the non-uniformity of the detector need to be accounted for?

## 5. Theory

After the data reduction, the intermediate scattering function shows a smooth decay as a function of time. A model must be fitted to the data to obtain the characteristic decay constant. The intermediate scattering function  $I(Q,t)/I(Q,0)$  may be expanded into cumulants [5,6]:

$$\frac{I(Q,t)}{I(Q,0)} = \exp \left[ - \left( c_1(Q)t + \frac{c_2(Q)t^2}{2!} + \frac{c_3(Q)t^3}{3!} \dots K \right) \right] \quad (15)$$

In simple cases the second and higher-order cumulants can be neglected, and the well-known result is:

$$c_1(Q) = D_{eff} Q^2 \quad (16)$$

where  $D_{eff}(Q)$  is the effective diffusion coefficient. Hence

$$\frac{I(Q,t)}{I(Q,0)} = \exp \left[ - D_{eff}(Q) Q^2 t \right] \quad (17)$$

If there is no internal dynamics, and hydrodynamic interactions can be neglected, the effective diffusion coefficient is given by:

$$D_{eff}(Q) = D_0 \frac{1}{S(Q)} \quad (18)$$

where  $D_0$  is the diffusion coefficient in the limit of infinite dilution (when there are no interactions) and  $S(Q)$  is the static structure factor. The hydrodynamic limit ( $Q \rightarrow 0$ ) of  $D_{eff}$  is the

translational diffusion coefficient,  $D_{tr}$ , that can be measured, for example, by dynamic light scattering. In the same hydrodynamic limit, at low volume fractions,  $S(0)$  can be described by a virial expansion, obtaining an approximate expression for the concentration dependence of the translational diffusion coefficient. In the limit of infinite dilution the Stokes-Einstein relation applies:

$$D_0 = \frac{k_B T}{6\pi\eta R_H} \quad (19)$$

where  $\eta$  is the solvent viscosity,  $k_B T$  is the thermal energy, and  $R_H$  is the hydrodynamic radius. For a smooth sphere  $R_H$  is equal to the true radius of the sphere. In reality,  $R_H$  is the radius of the diffusing entity: the real particle plus a somewhat extended hydration layer.

- How does  $R_H$  compare to  $R_g$  measured in a static experiment as SANS?

If the investigated sample is not a rigid sphere, some kind of internal dynamics may fall into our space-time window and contribute to the observed dynamics. In the specific case of our microemulsion, since only the surfactant has scattering contrast, the motions that are visible are the translation and undulations of the shell. Since we can assume that the two dynamics are not correlated we can write:

$$D_{eff}(Q) = D_{tr}(Q) + D_{def}(Q) \quad (20)$$

where  $D_{def}(Q)$  is a diffusion coefficient representative of the droplet shape deformations.

$D_{def}(Q)$  can be derived from an expansion of the shape fluctuations into spherical harmonics [3,7,8]:

$$D_{def}(Q) = \frac{5\lambda_2 f_2(QR_0) \langle |a_2|^2 \rangle}{Q^2 \left\{ 4\pi [j_0(QR_0)]^2 + 5f_2(QR_0) \langle |a_2|^2 \rangle \right\}} \quad (21)$$

with

$$f_2(QR_0) = [4j_2(QR_0) - QR_0 j_3(QR_0)]^2 \quad (22)$$

where  $\lambda_2$  is the damping frequency of the droplet deformation,  $j_n(x)$  is the  $n$ -th order spherical Bessel function,  $\langle |a_2|^2 \rangle$  is the mean square displacement of the 2<sup>nd</sup>-mode spherical harmonic ( $n=2$ ) and  $R_0$  is the mean droplet radius.

In order to relate our experimentally determined parameter  $\lambda_2$  to the modulus of elasticity of the AOT film we use the following equation [9]:

$$\lambda_2 = \frac{k}{\eta R_0^3} \left[ 4 \frac{R_0}{R_s} - 3 \frac{\bar{k}}{k} - \frac{3k_B T}{4\pi k} f(\phi) \right] \frac{24\eta}{23\eta' + 32\eta} \quad (23)$$

where  $k$  is the bending modulus of elasticity of the AOT film,  $k^-$  is the saddle-splay modulus of the AOT film,  $R_s$  is the spontaneous curvature of the AOT film,  $f(\phi)$  is the mixing entropy per droplet as a function of the volume fraction  $\phi$ ,  $\eta$  is the bulk viscosity of deuterated  $n$ -hexane (outside the droplets), and  $\eta'$  is the bulk viscosity of deuterated water (inside the droplets). Equation 23 must be combined with the following equation for the polydispersity,  $p$ :

$$p^2 = \frac{k_B T}{4\pi} \left[ 6(2k + k^-) - 8k \frac{R_0}{R_s} + \frac{3k_B T}{2\pi} f(\phi) \right]^{-1} \quad (24)$$

where  $p$  is defined as:

$$p = \sqrt{\frac{\langle R^2 \rangle}{\langle R \rangle^2} - 1}, \quad R_0 = \langle R \rangle \quad (25)$$

Finally, from equations 23 and 24 we obtain for the bending modulus of elasticity of the AOT film:

$$k = \frac{1}{48} \left[ \frac{k_B T}{\pi p^2} + \lambda_2 \eta R_0^3 \frac{23\eta' + 32\eta}{3\eta} \right] \quad (26)$$

After fitting  $I(Q,t)/I(Q,0)$  to a  $Q$ -dependent single exponential to determine  $D_{\text{eff}}(Q)$ , using equation 8 we can fit  $D_{\text{eff}}(Q)$  to obtain  $\lambda_2$  and  $\langle |a_2|^2 \rangle$  as fitting parameters. Then, using the polydispersity found from the SANS measurement, the bending modulus of elasticity of the AOT film,  $k$ , can be calculated.

- What does non-linear data on a plot of  $\ln\{I(Q,t)/I(Q,0)\}$  versus time tell you about the higher order cumulants?
- Why can't you measure the diffusion coefficient of individual micelles and the shape fluctuations of microemulsion droplets by using dynamic light scattering?
- What effect would size polydispersity have on the measured  $I(Q,t)$ ?
- Would you expect any  $Q$ -dependence of  $D_{\text{eff}}$  performing an experiment on AOT micelles?
- Can you see rotational motions of the spherical shell of the AOT microemulsion?
- Does the value of  $k$  make any sense?

## 5. Concluding remarks

This experiment involving an AOT microemulsion is similar to one of the first measurements ever performed on an NSE spectrometer using surfactants [10]. These early experiments were quite significant, however, to demonstrate that the behavior of colloidal fluids could be treated as an extension of simple atomic fluids. When the NSE experiments were originally performed (approximately 1980), this issue was under serious debate. In fact, there was not even agreement about the structure of a simple spherical micelle.

We can summarize that NSE spectroscopy is a well suited technique for the investigations of aperiodic relaxation dynamics. It covers a wide range of applications: in classical solid state physics, critical scattering in the fields of magnetism and structural phase transitions; in soft matter, polymers, glassy systems, and complex fluids such as micelles, microemulsion, or systems with biological relevance.

## 6. References

- [1] The present hand-out is largely an adaptation of the paper “Neutron Spin Echo Spectroscopy at the NIST Center for Neutron Research”, N. Rosov, S. Rathgeber, and M. Monkenbusch, *ACS symposium series*, **739**, 103 (2000).
- [2] Additional information on NSE can be found in *Neutron Spin Echo*; Editor, F. Mezei, Lecture Notes in Physics, **128**; Springer-Verlag: Berlin (1980); and *Neutron Spin Echo*; Editors, F. Mezei, C. Pappas, and T. Gutberlet, Lecture Notes in Physics, **601**; Springer-Verlag: Heidelberg (2003)
- [3] J. S. Huang, S. T. Milner, B. Farago, and D. Richter, *Physical Review Letters*, **59**, 2600 (1987).
- [4] M. Monkenbusch, R. Schätzler, and D. Richter, *Nucl. Instr. Meth. Phys. Res. A*, **399**, 301 (1997).
- [5] J. C. Brown, P. N. Pusey, J. W. Goodwin, and R. H. Ottewill, *J. Phys. A*, **8**, 664 (1975).
- [6] W. Hess and R. Klein, *Physica*, **94A**, 71 (1978).
- [7] H. B. Stuhrmann, *Acta Crystallogr. Sect A*, **26**, 297 (1969).
- [8] B. Farago, D. Richter, J. S. Huang, S. A. Safran, and S. T. Milner, *Physical Review Letters*, **65**, 3348 (1990).
- [9] Y. Kawabata, M. Nagao, H. Seto, S. Komura, T. Takeda, D. Schwahn, N. L. Yamada, and H. Nobutou, *Phys. Rev. Letters*, **92**, 056103 (2004).
- [10] J. B. Hayter and J. Penfold, *J. Chem. Soc., Faraday Trans. I*, **77**, 1851 (1981).

## Appendix A: Incoherent scattering measurements with NSE spectroscopy from Hydrogenous Samples

There are three sources of incoherent scattering: isotopic variation in the nuclear cross-section, uncorrelated motions, and variation in the nuclear cross section due to the nuclear spin. In the following of this appendix, we refer in particular to nuclear spin incoherence and specifically to hydrogenated samples.

With the classical NSE spectrometer design, it is possible to measure the nuclear incoherent intermediate structure factor  $I_{incoh}(Q,t)$  as well; however, in practice, some difficulties need to be overcome. Most importantly the incoherent scattering intensity is most of the times low. The incoherent scattering is spread out isotropically in a solid angle of  $4\pi$ , therefore its intensity is generally much lower than the intensity of coherent scattering, which is concentrated in a limited region of the  $Q$  space (consider for example how the SANS signal compares to the incoherent background).

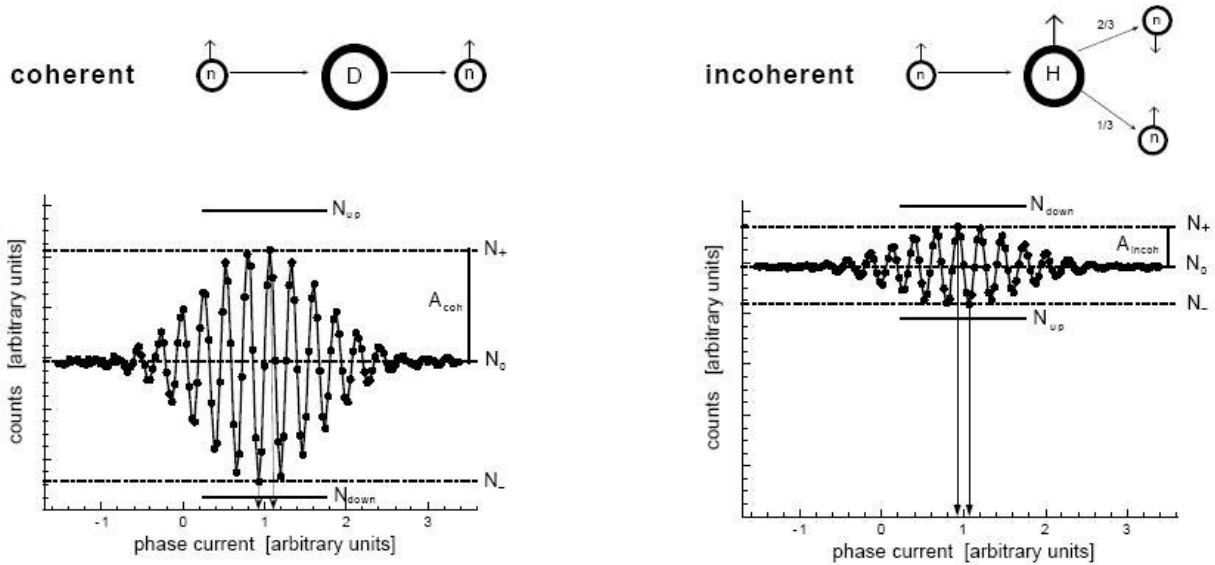


**Figure 6.** NSE signal as a function of the phase difference between the incident and scattered beams. The upper part of the figures shows the principle difference, in the case of deuterons and protons, between the scattering from a nucleus with and without nuclear spin. The lower part shows the NSE signals obtained in both cases – the count rate is plotted against the current of the phase correction coil.  $A_{coh}$  and  $A_{incoh}$  are the echo amplitudes for coherent and incoherent scattering,  $N_0$  is the average count rate outside the echo,  $N_+$  and  $N_-$  are the maximal and minimal

count rates with the  $\pi/2$ -flippers on, and  $N_{up}$  and  $N_{down}$  are the count rates of non spin flip ( $\pi$ -flipper off) and spin flip ( $\pi$ -flipper on) measurements made with the  $\pi/2$ -flippers off.

Moreover, the nuclear spin-incoherent scattering intrinsically reduces the polarization of the scattered beam, and therefore the echo amplitude, as shown in figure 6. Nuclear spin incoherence causes, with a nucleus dependent probability, a spin flip of both the inelastically and elastically scattered neutrons, e.g., 2/3 of the neutrons scattered from an H atom undergo a spin flip, whereas deuterium, which has no nuclear spin, has no influence on the neutron spin. In nuclear spin-incoherent scattering processes, some fraction of the neutron spins are flipped by  $180^\circ$  and produce an echo that is reversed with respect to the non-spin-incoherent case. The overall echo amplitude is a superposition of the signals with opposite sign from the spin-flipped and non-spin-flipped neutrons, and so is reduced. For scattering from protons, the final signal is -1/3 of the signal from the non-spin-incoherent scattering case; the background is strongly increased as well, reducing the signal-to-noise ratio considerably. In the ideal case a purely incoherent scatterer gives a flipping ratio ( $N_{up}/N_{down}$ ) of 0.5, whereas for coherent scattering flipping ratios of the order of ten are customary. If, in addition, there is some coherent scattering present, the spin-incoherent and coherent cross sections have opposite signs for the echo signal and so reduce the echo signal in a way that cannot be decomposed.

However, if the incoherent signal is strong enough, for example in the case of aqueous systems, the incoherent scattering can be measured. With respect to a measurement performed with a time-of-flight or a backscattering spectrometer, the main benefits are a better energy resolution and the advantage of working in the time domain. The main drawback is that each Q value as to be measured separately. In any case, long counting times are to be expected.

For these reasons the main application of NSE spectroscopy is still to measure the intermediate coherent scattering function  $I_{coh}(Q,t)$ , the coherent density fluctuations that correspond to some SANS intensity pattern. This type of scattering may be orders of magnitude more intense than the incoherent contributions. However, studies of the incoherent dynamics with NSE are possible and in some cases have been successfully performed in the past.

## Appendix B:

### Magnetic scattering measurements with NSE spectroscopy

You now know that the neutron spin echo technique is the neutron scattering method with the highest energy resolution. Relaxation times of several nanoseconds (corresponding to a resolution of the order of 100 neV) are easily measured and hence the technique is suited for slow dynamics. Although the majority of experiments done on a NSE spectrometer involve soft condensed matter, the technique is also very important in the study of magnetic samples with slow spin dynamics. By utilizing polarized neutrons, NSE allows the separation of magnetic and nuclear coherent and incoherent scattering.

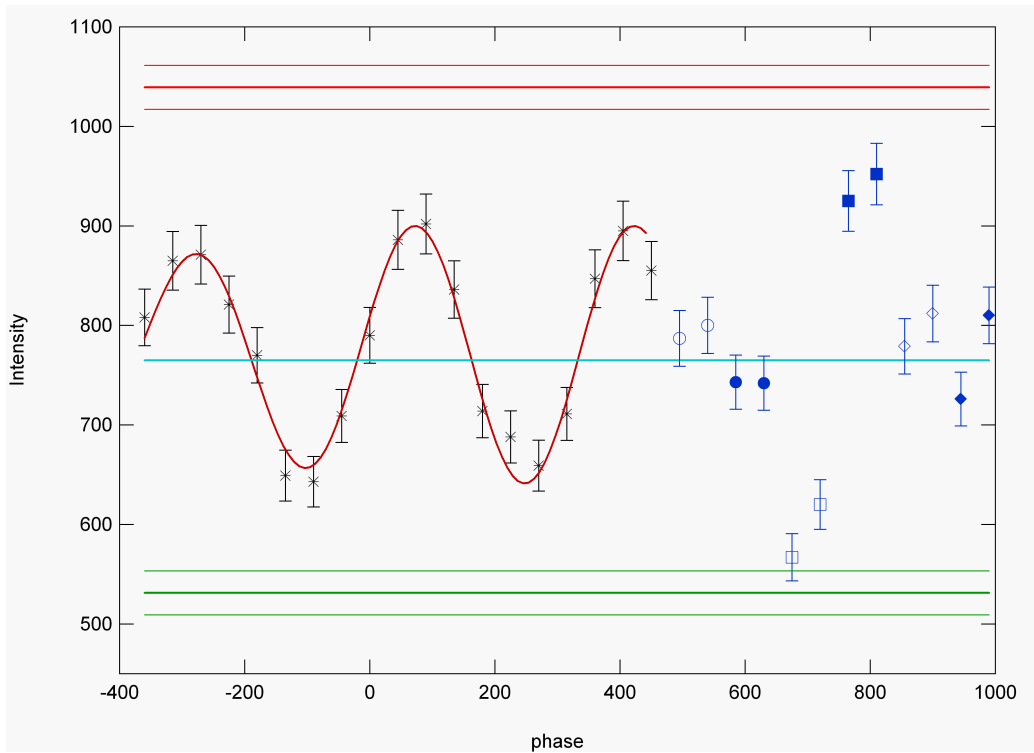


Fig. 7 Example of an echo measured for a magnetic signal. The last six points are the measurement of the xyz polarization. The open symbols refer to the down measurements (no spin inversion) and the closed symbols to the up measurements (spin inversion). x: circles; z: squares; y: diamonds. Note the ‘inversion’ for the z measurements: the up counts are much higher than the down. In fact, the magnetic intensity is:  $S^M(Q) = 2(z_{up} - z_{dwn}) - (x_{up} - x_{dwn}) - (y_{up} - y_{dwn})$ . The cyan line represents the average intensity:  $S(Q) = (z_{up} + z_{dwn} + y_{up} + y_{dwn} + x_{up} + x_{dwn})/6$ . The distance between the red and green line is the normalization factor for the magnetic echo and is equal to the magnetic intensity divided by 2.

In fact, in NSE experiments with magnetic samples one almost always employs three-directional neutron polarization analysis (often referred to as  $xyz$  polarization analysis) to measure the magnetic part of the static structure factor  $S(Q)$ . To do this the instrument is run in polarized diffraction mode without echo but with a  $\pi$  flipper. One measures six cross sections with the magnetic field along three axes  $x$ ,  $y$ , and  $z$  ('up' and 'down' for each).

Certain linear combinations of these cross sections cancel the nuclear coherent and incoherent scattering contributions, thus allowing the separation of the purely magnetic scattering, magnetic  $S^M(Q)$ . With polarized neutrons, one always identifies the magnetic scattering unambiguously.

During the echo experiment one takes advantage of the fact that a magnetic species does a  $\pi$  flip of the neutron (spin inversion). Therefore, one important difference between a magnetic experiment and the other experiments done on the spectrometer is the absence of the  $\pi$  flipper near the sample position. Therefore only the spin flipped neutrons contribute to the echo, whereas the nuclear scattering originates a depolarized background. The remaining experimental details are the same. The echo amplitude, which is purely due to magnetic scattering, is then normalized to the magnetic  $S^M(Q)$  obtained from the  $xyz$  polarization analysis.

The difficulties with magnetic NSE experiments include the weak signal, neutron depolarization from ferromagnetic components to the spin-correlations and the necessity for slow spin dynamics. The technique has however proven indispensable in spin-glass physics and frustrated magnetism.

## NSE at a glance

- Sensitive to the time-dependent density-density correlation function. Directly measures the intermediate scattering function  $I(Q,t)$ .
- Bridges the gap in time scale between conventional inelastic neutron scattering and dynamic light scattering. ( $Q$ -range of  $0.01\text{--}1.6\text{\AA}^{-1}$  and Fourier times of up to  $10^{-7}$  s available.)
- NIST spectrometer is optimized for measurements of **soft condensed matter** systems. For example:

### **Polymers**

Observation and quantitative description of the crossover in dynamics from local segmental diffusion to time-dependent behavior governed by entanglements occurring over longer length scales.

### **Glassy dynamics**

Identification in polymer glasses of the intra- and inter- molecular dynamics responsible for the  $\alpha$  and  $\beta_{\text{slow}}$  relaxation.

### **Biological model systems**

Quantitative description of the effect of interlayer coupling in the extended diffusive mode of lipid bilayers.

### **Proteins**

Intra-molecular diffusion in *e.g.*, pig immunoglobulin G.

- By using polarized neutrons, provides an intrinsic separation of magnetic and nuclear scattering, making data analysis easy and the interpretation unambiguous for this kind of experiments.

---

## Present Spectrometer Operating Characteristics

- Scattering angle up to  $105^\circ$ ;  $Q_{\text{max}} = 1.25\text{\AA}^{-1}$  for  $8\text{\AA}$ .
- $Q_{\text{min}}$  and  $Q$ -resolution  $< 0.02\text{\AA}^{-1}$ .
- Polarized beam available for wavelengths  $> 5\text{\AA}$ .
- Maximum Field integral  $|B|dl = 0.438\text{ T}\cdot\text{m}$  (40 ns at  $8\text{\AA}$ ).
- $2 \times 10^6\text{ n/cm}^2/\text{s}$  at  $8\text{\AA}$  (10% FWHM wavelength distribution).
- Typical sample size:  $3 \times 3\text{cm}^2$ .